

UC Irvine

UC Irvine Previously Published Works

Title

Optimal wavelength for ultrahigh-resolution optical coherence tomography.

Permalink

<https://escholarship.org/uc/item/36p568zz>

Journal

Optics express, 11(12)

ISSN

1094-4087

Authors

Wang, Yimin
Nelson, J
Chen, Zhongping
et al.

Publication Date

2003-06-01

DOI

10.1364/oe.11.001411

Peer reviewed

Optimal wavelength for ultrahigh-resolution optical coherence tomography

Yimin Wang, J. Stuart Nelson, Zhongping Chen

Beckman Laser Institute, University of California, Irvine,
1002 Health Sciences Road East, Irvine, CA 92612
Zchen@laser.bli.uci.edu

Bibiana Jin Reiser, Roy S. Chuck

Department of Ophthalmology, University of California, Irvine, CA 92697

Robert S. Windeler

OFS Laboratories, 600 Mountain Avenue, Murray Hill, NJ 07974

Abstract: The influence of depth dependent dispersion by the main component of biological tissues, water, on the resolution of OCT was studied. Investigations showed that it was possible to eliminate the influence of depth dependent dispersion by water in tissue by choosing a light source with a center wavelength near 1.0 μm . Ultrahigh resolution ophthalmic imaging was performed at this wavelength range with a microstructure fiber light source.

© 2003 Optical Society of America

OCIS codes: (110.4500) Optical Coherence Tomography; (170.1650) Coherence Imaging; (170.3800) Medical and biological imaging

References and links

1. D. Huang, E. Swanson, C. P. Lin, J. S. Schuman, W. G. Stinson, W. Chang, M. R. Hee, T. Flotte, K. Gregory, C. A. Puliafito, and J. G. Fujimoto, "Optical coherence tomography," *Science* **254**, 1178-1181 (1991).
2. R. C. Youngquist, S. Carr, and D. E. N. Davies, "Optical coherence-domain reflectometry: a new optical evaluation technique," *Opt. Lett.* **12**, 158-160 (1987).
3. W. Drexler, U. Morgner, F. X. Kartner, C. Pitris, S. A. Boppart, X. D. Li, E. P. Ippen, and J. G. Fujimoto, "In vivo ultrahigh-resolution optical coherence tomography," *Opt. Lett.* **24**, 1221-1223 (1999).
4. J. K. Ranka, R. S. Windeler, and A. J. Stentz, "Visible continuum generation in air-silica microstructure optical fibers with anomalous dispersion at 800nm," *Opt. Lett.* **25**, 25-27 (2000).
5. I. Hartl, X. D. Li, C. Chudoba, R. K. Ghanta, T. H. Ko, and J. G. Fujimoto, "Ultrahigh-resolution optical coherence tomography using continuum generation in an air-silica microstructure optical fiber," *Opt. Lett.* **26**, 608-610 (2001).
6. Christoph K. Hitzenberger, Angela Baumgartner, Wolfgang Drexler, and Adolf F. Fercher, "Dispersion effects in partial coherence interferometry: implications for intraocular ranging," *J. of Bio. Opt.* **4**, 144-151 (1999).
7. J. F. de Boer, C. E. Saxer, and J. S. Nelson, "Stable carrier generation and phase-resolved digital data processing in optical coherence tomography," *Appl. Opt.* **40**, 5787-5790 (2001).
8. E. D. J. Smith, A. V. Zvyagin, and D. D. Sampson, "Real-time dispersion compensation in scanning interferometry," *Opt. Lett.* **27**, 1998-2000 (2002).
9. B. L. Danielson and C. Y. Boisrobert, "Absolute optical ranging using low coherence interferometry," *Appl. Opt.* **30**, 2975-2979 (1991).
10. Amelia G. Van Engen, Scott A. Diddams, and Tracy S. Clement, "Dispersion measurements of water with white-light interferometry," *Appl. Opt.* **37**, 5679-5686 (1998).
11. P. Schiebener, J. Straub, J. M. H. Levelt Sengers and J. S. Gallagher, "Refractive index of water and steam as function of wavelength, temperature and density," *J. Phys. Chem. Ref. Data* **19**, 677-717 (1990).
12. Y. Wang, Y. Zhao, J. S. Nelson, Z. Chen, and R. S. Windeler, "Ultrahigh-resolution OCT using broadband continuum generation from a photonic crystal fiber," *Opt. Lett.* **28**, 182-184 (2003).
13. J. H. Chang, H. Ren, W. M. Petroll, H. D. Cavanagh and J. V. Jester, "The application of in vivo confocal microscopy and tear LDH measurement in assessing corneal response to contact lens and contact lens solutions," *Cur. Eye Res.* **19**, 171-181 (1999).

1. Introduction

Optical coherence tomography (OCT) is a noninvasive technology currently used to perform *in vivo* high-resolution, cross-sectional imaging of microstructure in biological tissues [1]. By measuring singly back scattered light as a function of depth, OCT has the potential to image tissue structure with high resolution and sensitivity *in vivo*. Coherence-domain ranging in OCT is performed using a Michelson interferometer. Longitudinal resolution, governed by the source coherence length, is inversely proportional to the light source bandwidth. Superluminescent diodes (SLD) are often used for OCT imaging and typically have 10-15 μm longitudinal resolution [2] due to limited optical bandwidth. A Kerr-lens mode-locked Ti:sapphire laser, optimized for a short coherence length, can obtain longitudinal resolution of less than 2 μm [3]. Recent developments in optical fiber technology permit an extremely broadband continuum light spectrum to be extracted from highly nonlinear microstructure fibers [4]. Longitudinal resolution of 2.5 μm was reported with a microstructure fiber light source at a wavelength of 1.3 μm [5]. With the advances in light source technology, longitudinal resolution has been improved significantly since OCT was first applied to image the microstructure of the eye.

With the improvement in OCT resolution due to increased source bandwidths, one potential limitation that arises is the dispersion of the sampling medium. Depth dependent dispersion is a limitation when scanning across a long distance, such as in the eye. Generally, OCT systems require adjustment of the dispersion balance between the two arms of the interferometer [6]. However, this compensation works only for one plane, which prevents high axial resolution over the entire scanning depth. For ultrahigh resolution OCT, any unbalanced dispersion in the interferometer may degrade axial resolution, and dynamic dispersion compensation is needed for deep imaging depth. Postprocessing based compensation of OCT images with known scanning independent dispersion imbalance has been demonstrated [7]. However, such compensation requires significant data processing. By tilting the grating in the frequency domain optical delay line (FD-ODL), it is possible to obtain depth dependent dispersion [8]. But the limited bandpass of FD-ODL makes it difficult to be used in ultra-high resolution OCT. In this paper, the influences of depth dependent dispersion by the main component of biological tissues, water, on the resolution of OCT were investigated. Studies showed that it was possible to eliminate the influence of depth dependent dispersion in tissue of water by choosing a light source with a center wavelength near 1.0 μm . We developed an ultra broadband light source at this wavelength and performed ophthalmic imaging with a longitudinal resolution of 1.3 μm .

2. Analysis

In a Michelson interferometer, light traveling a distance z through a dispersion sample will cause a phase shift to be introduced into the back scattered interferogram $\phi(\omega)$. Theoretical analysis has shown that for a light source with a Gaussian spectrum, the width of the field autocorrelation function increases according to [9]:

$$\sigma_t = \sigma_{t0} \left\{ 1 + \left[\frac{d^2 \phi(\omega)}{d\omega^2} \right]^2 \sigma_\omega^4 \right\}^{1/2} \quad (1)$$
$$K = \sigma_t / \sigma_{t0}$$

with the group velocity dispersion (GVD) D defined as

$$D = \frac{-\omega_0^2}{2\pi c} \frac{d^2 \phi(\omega)}{d\omega^2} \quad (2)$$

where σ_t is the $1/e^{1/2}$ half width of the autocorrelation function, and σ_{t0} is the $1/e^{1/2}$ half width of the autocorrelation function when D is zero. The $1/e^{1/2}$ half width of the light spectrum is σ_w , and ω_0 is the central frequency of the light spectrum. K is the broadening ratio. Equation (1) shows that the wider the source bandwidth, the more sensitive the measurement is to GVD. However, if a suitable optical wavelength is chosen such that $D=0$, the depth dependent broadening of the autocorrelation function will be eliminated.

The common constituents of biological tissues are water and hemoglobin. Water constitutes about 60% in normal tissues and higher in some anatomic structures, such as 90% in the eye. Thus, the dispersion of water greatly influences the dispersion characteristics of biological tissue, especially during ophthalmic imaging. In our experiment, the dispersion of water was measured by analyzing interference fringes from a Michelson interferometer [10]. Because the refractive index of water is temperature dependent [11], we measured the dispersion of water at 37°C, not at 20°C as in Ref. [10]. Continuum light from a microstructure fiber was chosen as the light source to perform this measurement. The measured result of water dispersion is shown in Fig. 1 as the triangle symbols. The solid line in Fig. 1 is the calculated result, and the refractive index of water for this calculation is from Ref. [11]. From Fig. 1, it can be noted that for traditional OCT light sources, 800 nm and 1.3 μm , the dispersion D of water is nonzero. According to Eq. (1), this nonzero dispersion leads to broadening of the interference fringes

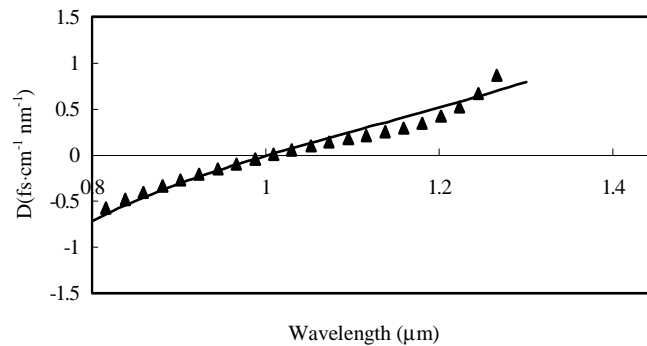


Fig. 1. Chromatic dispersion of water. Triangles: experimental result; solid line: calculated result.

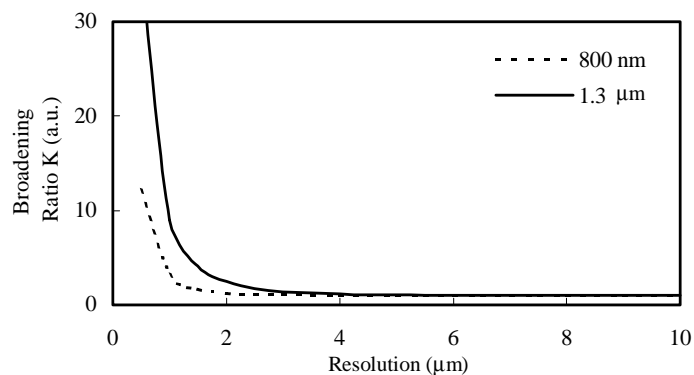


Fig. 2. Broadening effect for different OCT resolutions. K is the ratio of coherence length with and without water dispersion. Dashed line: 800 nm light source; solid line: 1.3 μm light source.

and a decrease in resolution when 800 nm or 1.3 μm light sources are used for OCT imaging of biological tissues. Figure 2 shows the calculated broadening of the autocorrelation function due to nonzero dispersion with Eq. (1). The horizontal axis shows OCT resolution which is determined by the source bandwidth. The vertical axis is the broadening ratio K for the autocorrelation function from light before and after passing through a 1 mm thick water sample. It can be noted that for low OCT resolution, such as 10 μm , the broadening effect is small in which the influence of dispersion on OCT resolution can be ignored. However, with increasing resolution, K also increases. When the OCT resolution is smaller than 2 μm , K increases steeply. As a result, the width of the autocorrelation function is broadened greatly after light passing through the water sample, and the OCT resolution is seriously degraded. Thus, for OCT imaging with a resolution smaller than 2 μm , dynamic dispersion compensation is needed even for a small imaging depth.

From the curve in Fig. 1, it can be noted that the zero dispersion wavelength of water is near 1.0 μm . Theoretical calculations showed that from 20 $^{\circ}\text{C}$ to 37 $^{\circ}\text{C}$, the zero dispersion wavelength of water is shifted from 1.0007 μm to 1.0026 μm . Thus, if the center wavelength of the OCT light source is chosen near 1.0 μm , the influence of depth dependent dispersion can be eliminated. An experiment was performed to compare the broadening effect of several different OCT SLD sources at 940 nm and 1.32 μm with spectrum widths of 75 nm and 76 nm, respectively. Because there was no wideband SLD source at 1.0 μm that was available, we chose the SLD source at 940nm to demonstrate the broadening effect at a wavelength near 1.0 μm . The broadening ratios, K , of autocorrelation function as a function of water thickness for two wavelengths were measured. In Fig. 3, the triangle and cross symbols are the experimental data for 1.32 μm and 940 nm, respectively, and the solid lines are the calculated results. From Fig. 3, it can be noted that with increasing water thickness, the broadening effect of the 1.32 μm source is much greater than that of the 940 nm source. This experimental result shows that the light source near 1.0 μm had a small GVD and that its influence on OCT resolution is much smaller than at 1.3 μm . To simulate the broadening effect in ultrahigh resolution OCT, calculations were done to compare the different broadening effects for ultra wideband light sources at 800 nm, 1.0 μm , and 1.3 μm . Spectrum widths for these three sources were 282, 441, and 746 nm, respectively, to satisfy 1.0 μm longitudinal resolution. The calculated results are shown in Fig. 4 where it can be noted that, after passing through 300 μm thickness of water, the interference fringes for the 800 nm and 1.3 μm sources broadened rapidly. Therefore, if the 800 nm or 1.3 μm light source is used, the performance of

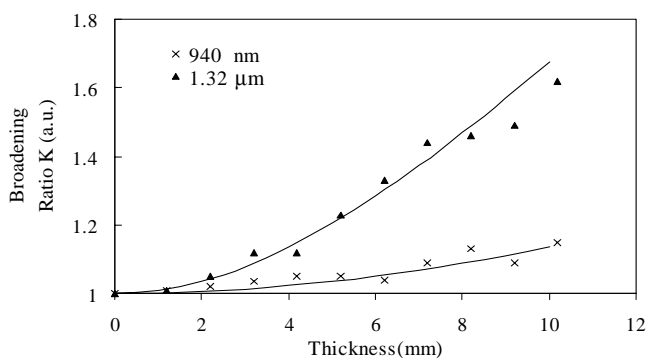


Fig. 3. Broadening of autocorrelation function when light passes through water sample. The light sources are at 940 nm and 1.32 μm .

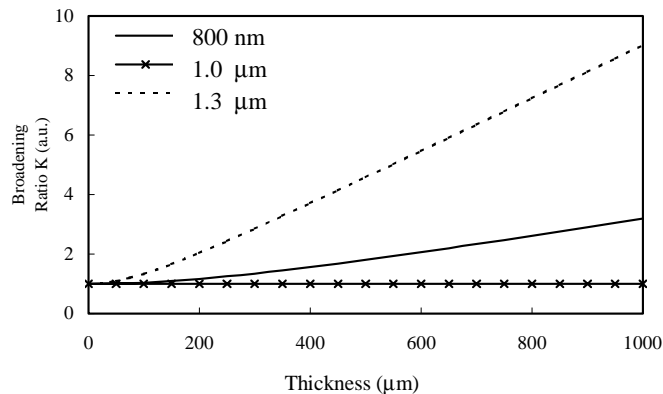


Fig. 4. Calculated broadening effects for broadband light sources at center wavelengths of 0.8, 1.0, and 1.3 μm , respectively. The bandwidths were chosen such that the longitudinal resolution was maintained at 1.0 μm .

ultrahigh resolution OCT will be degraded significantly with deeper imaging depths due to the dispersion by water in tissue. However, with a 1.0 μm light source, the OCT can maintain high resolution to a larger depth range.

3. Experiment

To demonstrate the advantage of employing a low dispersion light source for ultrahigh resolution OCT imaging, we developed a light source with an ultrawide spectrum from 800 nm to 1.4 μm from a microstructure fiber with a center wavelength at 1.1 μm [12]. The pump source for the microstructure fiber is a self mode-locked Ti:sapphire laser at 780 nm. The pump power from the laser is 650mW with a pulse duration of 110 fs and a repetition rate of 76 MHz. The output power from the microstructure fiber was approximately 50 mW after an 800 nm long pass filter. An open-air, ultrahigh resolution OCT system was designed and constructed in our experiment. A dynamic focusing method was used to increase imaging depth with constant lateral resolution. Our OCT system was optimized to support 1.3 μm longitudinal resolution in biological tissues [12]. The lateral resolution of the system was 7 μm , which was determined by the achromatic objective lens. The anterior chamber of the rabbit eye was imaged *in vitro*. The sample was a New Zealand white rabbit eye which was enucleated within 3 hours of death. The globe was stored in a moist chamber at 4⁰C until time of use. The central and limbal regions of the eye were scanned.

Figure 5(a) shows the image of the corneal epithelium at the center of the eye. The image size is 0.3 x 0.2 mm. The measured epithelium thickness is approximately 45 μm which correlates with reported results [13]. Figure 5(b) shows an image of the anterior chamber at the limbus of the eye to visualize the inner structures. The scanning rate of the moving stage was 2Hz. It took about 3 minutes to get one image. The whole image depth is 1.74 mm, which has been calibrated by the refractive index in the eye. The measured epithelium thickness at limbus is about 39 μm , thinner than the thickness at center part. I_1 is the interface between the epithelium and stroma, and I_2 is the interface between the endothelium and aqueous humor. The cornea, iris, and conjunctiva can be clearly visualized. The interface between the aqueous humor and lens, I_3 , is delineated. The width of the line at I_3 shown on the image is uniform from left to right. We compared the width of the interference peaks at I_3 with and without light passing through the iris, and there was no difference between them. To investigate the evolution of the OCT resolution with increasing imaging depths inside the eye, the envelope

of the interference peaks at line A-A in Fig. 5(b) was derived and is shown in Fig 5(c). Because the intensity of the interference peak at the front surface is about 100 times higher than the peak intensity from the structures inside the eye, we chose the interface, I_1 , as a

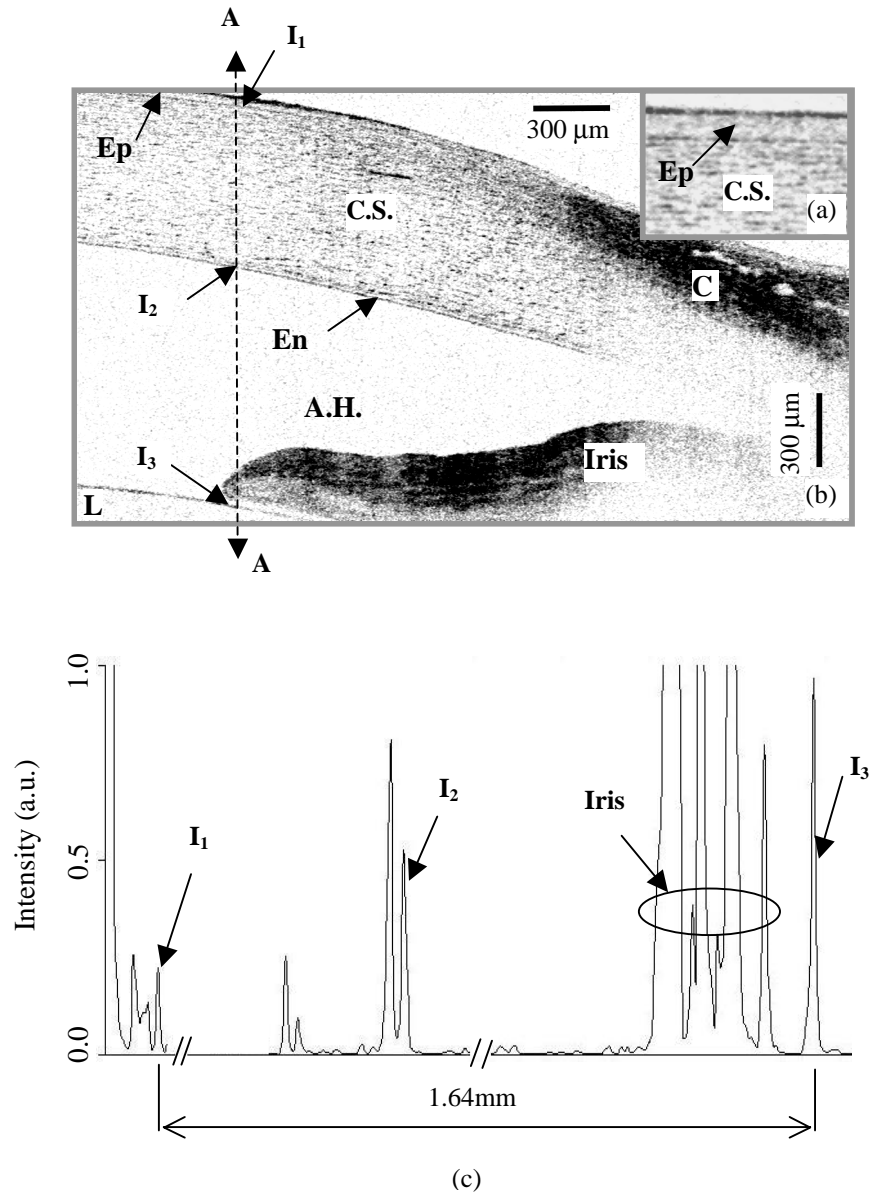


Fig. 5. High resolution ophthalmic imaging. (a) Cornea: image size 0.3 x 0.2 mm ; Ep, epithelium; C.S., corneal stroma. (b) Anterior chamber of eye: image size 3.0 x 1.74 mm; En, endothelium; A.H., aqueous humor; C, conjunctiva; L, lens; I_1 , interface between epithelium and stroma; I_2 , interface between endothelium and A.H.; I_3 , interface between A.H. and lens. (c) Interference peaks at line A-A in (b).

reference. The measured width of the interference peak at I_3 was 1.3 times of the width at I_1 because the center wavelength of our light source was at $1.1 \mu\text{m}$, not at $1.0 \mu\text{m}$ exactly, and the influence of dispersion still existed. Table 1 shows the broadening ratio K of interference peaks at difference depth I_2 and I_3 in the eye. L is the distance of I_2 and I_3 from interface I_1 . Comparing the width of the interference peak at I_2 and I_3 with that at I_1 , we can see that the resolution of the OCT is not degraded after light passes through 1.64 mm thickness of cornea, aqueous humor, and iris inside the eye. This demonstrates that high resolution is kept in a great depth range. Thus, a source near $1.0 \mu\text{m}$ is very promising for ultrahigh resolution OCT in biomedical imaging. Furthermore, selecting a wavelength of light with zero dispersion is a convenient way to eliminate the influence of the depth dependent dispersion in tissue compared with hardware methods.

Table 1. Broadening ratio K at different imaging depth

	L (mm)	K
I_2	0.6	1.1
I_3	1.64	1.3

4. Conclusion

In summary, the influences of the dispersion of the main component of biological tissue, water, on the resolution of OCT were studied. Investigations showed that by choosing a light source with a center wavelength near $1.0 \mu\text{m}$, it was possible to eliminate the influence of depth dependent dispersion of water in tissue. Ultrahigh resolution ophthalmic imaging was performed near this wavelength range with a microstructure fiber as the light source.

Acknowledgments

This work was supported by research grants awarded from the National Science Foundation (BES-86924) and National Institutes of Health (EB-00293, NCI-91717, EB-00255, RR-01192). Institute support from the Air Force Office of Scientific Research (F49620-00-1-0371) and the Beckman Laser Institute Endowment is also gratefully acknowledged.